SMAR 2019 – Fifth Conference on Smart Monitoring,
Assessment and Rehabilitation of Civil Structures

SMAR 2019

FE-Modelling Techniques for Structural Capacity Assessment of Corroded Reinforced Concrete Structures.

Alexander KAGERMANOV [1], Ivan MARKOVIC [1]

[1] University of Applied Sciences of Eastern Switzerland (HSR Hochschule für Technik Rapperswil), Rapperswil, Switzerland

Contact e-mail: ivan.markovic@hsr.ch

ABSTRACT: About 80% of the observed damage in existing concrete structures is related to reinforcement corrosion. Typical corrosion-associated phenomena that affect structural capacity concern: (i) cross-section and ductility reduction of steel, (ii) concrete cracking, (iii) concrete area reduction due to spalling and (iv) modification of the bond properties. A number of models have been presented in recent years addressing these issues. The paper presents a critical review of such models and its application to the analysis of corroded RC members using nonlinear FEA. The accuracy of different modelling approaches is assessed through comparison with experimental results on corroded beams subjected to monotonic loading. In addition, sensitivity studies are performed in order to gain better understanding of the contribution of each phenomenon. Final recommendations are given for reliable capacity assessment of existing structures affected by corrosion.

1 INRODUCTION

Most of existing structures, even if not located in particularly aggressive environments, suffer from carbonation and/or chloride attack over its life-span resulting in some level of corrosion. Field inspections on European bridge infrastructure report that about 70% of observed deterioration is related to corrosion [Gehlen et al. (2014)]. Meanwhile, several experimental and theoretical studies have pointed out the detrimental effects of corrosion-induced deterioration on the structural capacity [Rodriguez et al. (1996), Castel et al. (2000), Hanjari et al. (2011)], among others. However, the influence of corrosion is not always taken into account at ultimate limit state assessment, despite the fact that design codes require using updated material properties for verification of existing structures [e.g. SIA269]. Corrosion is typically regarded a durability issue that is limited to verifying the critical chloride content and carbonation front penetration.

In the case of nonlinear finite element analysis (NLFEA), the effects of corrosion can be accounted for through modification of the non-corroded material properties of steel, concrete and bond [Coronelli and Gambarova (2004)]. However, these modifications are not straightforward. Different models have been proposed in the last decades, which are usually derived from isolated experiments on a material level under accelerated corrosion. Their interaction, accuracy and numerical stability on a member level needs further investigation in order to provide unified modelling criteria for practical applications.

The paper presents an overview of the available models for corrosion-induced damage and their application to NLFEA. Experiments on corroded and non-corroded beam specimens subjected to 4 point bending were used as a benchmark. Models with varying levels of complexity were defined in order to gain better understanding of the contribution of each mechanism and its

influence on the collapse load and mode. Finally, recommendations are given for reliable capacity assessment of existing structures affected by corrosion.

2 MODELS FOR CORROSION-INDUCED DETERIORATION

2.1 Steel

2.1.1 Uniform and local corrosion.

Cross-section reduction of steel is the most relevant effect of corrosion. It initiates once the passive layer around the reinforcement is destroyed by carbonation and/or chloride penetration, causing uniform and localized (pitting) corrosion (Fig.1). Uniform corrosion can be directly accounted for in the analysis thorough reduction of the bar diameter as:

$$d_c=d_o-2x \quad (1)$$

where d_c is the corroded and d_o the initial bar diameter, and x the corrosion attack penetration. Attack penetration can be obtained either from direct measurements or estimated using analytical models for corrosion progression. Modeling corrosion progression in real structures is more challenging due to uncertainties in the large number of factors affecting corrosion, e.g. corrosion rate, type of corrosion products and environmental conditions, among others [Angst 2018].

Pitting corrosion varies randomly along the reinforcement, forming at imperfections in the passive layer. It is quantified with a pitting factor, R, representing the ratio between maximum pit depth, p, and average corrosion penetration calculated indirectly from weight loss. Typical R values for naturally corroded specimens vary between 4 and 8, and between 5 and 13 for accelerated corrosion [Gonzalez et al. (1995)]. Some probabilistic models have been proposed predicting the maximum pit depth as a function of the time of corrosion exposure, reinforcing bar diameter and bar length [Darmawan and Stewart (2006)]. However, it is a common assumption to localize pitting corrosion at critical sections such as mid-span or supports regions, thus neglecting spatial variability. The pit configuration is approximated with an equivalent circle of radius equal to the maximum penetration depth (Fig.1). Analytical expressions are provided in [Val and Melchers (1997)].

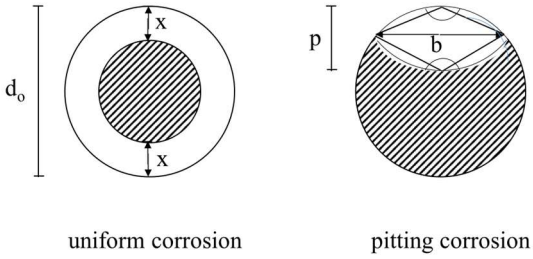

Figure 1: Modelling schemes for uniform and pitting corrosion of single reinforcement bar (effective cross-section of the corroded bar equals to the shaded area).

2.1.2 Mechanical properties.

It is generally agreed that corrosion causes ductility reduction of steel, i.e. reduction in the tensile fracture strain. However, some experimental tests show that yield and maximum stress remain unaffected [Apostolopoulos and Papadakis (2008)]. Theoretically, this corresponds to the case when corrosion is completely due to uniform corrosion. In the presence of pitting corrosion, however, there is a reduction in the yield and maximum stresses. Experimental observations suggest a linear relationship for strength and ductility reduction as follows [Cairns et al. 2005]:

$$X_c=(1-\alpha Q_c)X_o \quad (2)$$

where X_c, X_o is either yield stress f_y, maximum stress f_{max} or ultimate strain ε_u of corroded and un-corroded steel, respectively. Q_c is the percentage of cross-section loss due to pitting corrosion. Suggested values for α vary between 0.005-0.017 for f_y, between 0.010-0.018 for f_{max}, and between 0.000-0.060 for ε_u [Morinaga (1996), Cairns et al. (2005), among others]. This significant scatter is attributed to differences in the experimental techniques. Also, in some cases it is unclear whether the un-corroded or mean corroded area was used in the stress calculation. Larger α values could be associated with the un-corroded area, and therefore α would account for both uniform and pitting corrosion. Regarding the mode of failure, also different conclusions have been reported. In some cases yielding with ductility reduction was observed, whereas in others brittle fracture occurred after only 20% section loss [Stewart and Al-Harthy (2008)].

Figure 2 (left) shows the effect of pitting corrosion on the tensile yield capacity (yield stress × area) of reinforcement for different levels of normalized pit depth and α values. Also shown is the cross-section reduction. Since pitting corrosion affects both cross-section and yield stress, the relationship between yield capacity and cross-section loss is quadratic. For normalized pit depths of less than 10%, the loss in yield capacity is relatively small, as well as the influence of α. For larger pit depths, α values greater than 0.005 lead to excessive loss of yield capacity when the corroded cross-section is used in the calculation. It is therefore suggested to use α=0.005 when the cross-section is explicitly reduced in the model. In this case, it can be seen that most of the contribution to the yield capacity loss is due to the cross-section reduction.

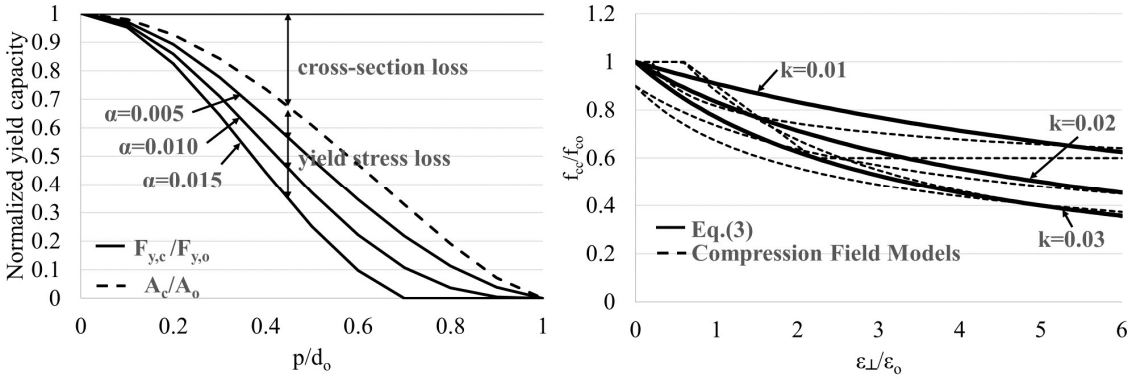

Figure 2. Normalized yield capacity due to pitting corrosion for different values of α (left), concrete compressive strength reduction due to corrosion cracking and comparison with compression field models (right).

2.2 Concrete

2.2.1 Compressive strength.

Tensile strains orthogonal to the direction of principal compression can cause reduction in the compressive concrete strength. This phenomenon, known as compression softening, has been previously observed for members in biaxial stress conditions within the context of compression field models [Vecchio and Collins (1986)]. Corrosion-induced cracks orthogonal to the compression field, e.g. cracks parallel to the compression reinforcement, can produce a similar effect, which has been also quantified as a function of the orthogonal tensile strain as [Coronelli and Gambarova (2004)]:

$$f_{cc}=\frac{f_{co}}{1+k\frac{\varepsilon_\perp}{\varepsilon_o}} \quad (3)$$

$$\varepsilon_{\perp}=\frac{nw_{cr}}{b_o} \quad (4)$$

where k is a factor related to bar diameter and roughness, ε_o is the strain at peak compressive stress, $\varepsilon_{\perp}$ is the smeared orthogonal tensile strain estimated as a function of the number of cracks, n, the average crack width for each bar, w_{cr}, and the member width b_o. Figure 2 (right) compares equation (3) with different expressions proposed in the context of compression field models [Belarbi and Hsu (1995)]. A similar overall trend can be observed, with k between 0.1-0.3 covering most of the range. For k=0.1, as proposed in [Coronelli and Gambarova (2004)] for medium-diameter ribbed bars, equation (3) yields less conservative reductions. It should be noted that in the case of corrosion, tensile strains occur in the circumferential direction due to internally restrained volume expansion, whereas compression field expressions were derived from biaxial panel testing (plane stress conditions) under direct loading. Although strictly speaking the two phenomenon are different, equation (3) represents a valuable approximation for practical applications.

The main challenge, however, relies in the estimation of w_{cr}. Different, usually linear, expressions have been proposed to quantify w_{cr} as a function of corrosion penetration. Figure 3 (left) compares two common expressions: (i) Molina et al. (1993), who proposed an analytical expression as a function of the volumetric expansion ratio, and (ii) Vidal et al. (2004), who proposed an empirical expression including the influence of bar diameter and concrete cover. Significant differences between the two approaches can be observed. The effect on the concrete compressive strength is shown in Figure 3 (right). For a corrosion penetration of 1mm, crack widths vary between 2 and 6mm. As a consequence, strength reductions range between 0.60 and 0.80. This difference is presumably related to the method of corrosion, which was accelerated corrosion in Molina et al., and natural corrosion in Vidal et al. Empirical expressions derived from accelerated corrosion tests result in larger crack widths and therefore in more conservative results.

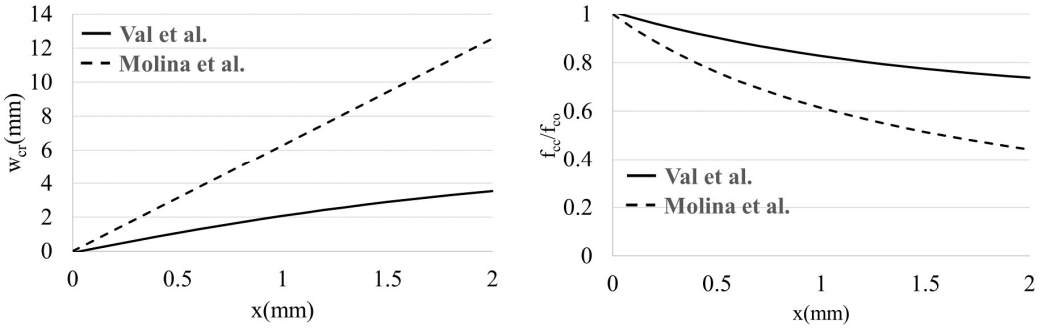

Figure 3. Corrosion-induced crack width as a function of corrosion penetration for Val et al. and Molina et al. models (left) and corrosion-induced compressive strength reduction according to equation (3) (right).

2.3 Bond

Corrosion generates flaky rust products around the rebar that affect bond adhesion and friction with surrounding concrete. A number of empirical models have been proposed usually based on pull-out tests of corroded bars with different diameters, concrete cover and presence of transverse reinforcement [fib (2000)]. It was shown that bond strength increases at early corrosion stages due to volume expansion and friction. Afterwards, a rapid loss of bond strength occurs until reaching a residual value which remains approximately constant (Fig.4 (left)).

Some models are compared in Figure 4 (right) [Val et al. (1998), Chung et al. (2004), Maddawy et al. (2005), Feng et al. (2006), Lundgren et al. (2009), Fischer (2012)], where the ratio between

maximum corroded and non-corroded bond strengths, *r*, is shown as a function of the weight loss. Most of the proposed models neglect the initial increase in bond strength and only consider the degrading phase. Differences between models are mostly due to the experimental data used for calibration, which is affected by the test set-up, specimens and current densities applied to accelerate corrosion.

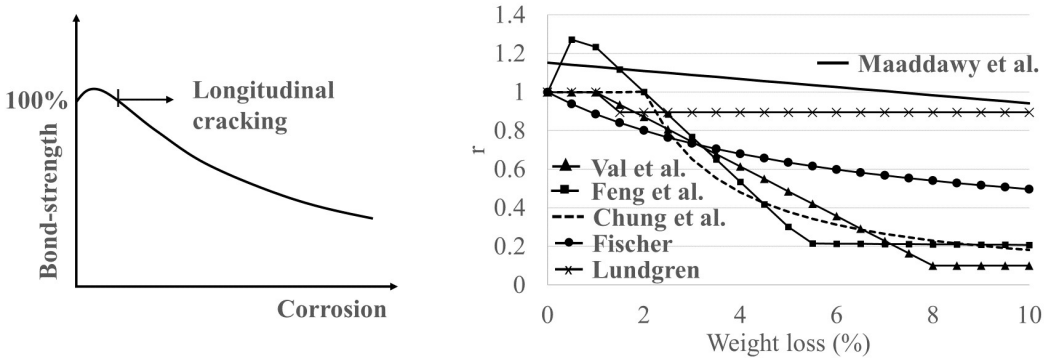

Figure 4: *Left*: Reduction of bond strength between reinforcement and concrete (adapted from [fib (2000)]) as a function of corrosion; *Right*: comparison between used models for bond reduction, with *r* being the ratio between maximum bond strengths in corroded and non-corroded state.

3 NON-LINEAR FINITE ELEMENT ANALYSIS.

Two beam specimens tested by Rodriguez et al. were selected for analysis. The specimens consisted of simply supported rectangular RC beams loaded in 4-point bending. Beam B111 was non-corroded, whereas beam B116 was corroded under accelerated corrosion. Further information on material and geometrical properties can be found in [Rodriguez et al. (1997)].

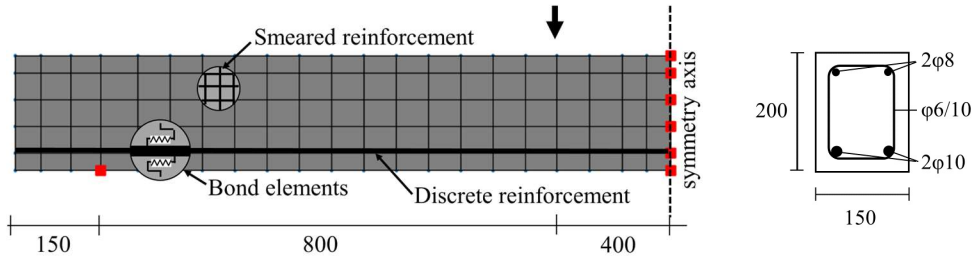

Figure 5. FE Model of RC beam with corroded reinforcement (based on experiments of Rodriguez et al.): geometry and cross-section layout (in mm), FE-computations were performed with the in-house IDEEA-FEM-Software for non-linear FEM-computations.

FE-Modelling was performed with IDEEA non-linear FEM-Software, which is available at HSR as an in-house FEM-software package. Given the symmetry conditions, only half of the beam was modeled with 105 plane stress (membrane) FE elements (Fig.5). Bottom flexural reinforcement was defined as discrete with nonlinear truss elements connected to concrete with bond elements. Top flexural and transverse reinforcement were defined as smeared with equivalent reinforcement ratios. An orthotropic, smeared-fixed-crack constitutive model was used for concrete. Steel was modeled with a uniaxial bilinear material model.

In order to quantify the contribution of each damage mechanism, models with increasing degree of complexity were defined. Modifications to the non-corroded FE model of beam B111 were successively introduced starting from uniform corrosion and adding the effects of pitting corrosion, yield strength reduction, etc. according to Table 1.

Model	Steel			Concrete		Bond	Comments
	U	P	f_y	f_c	C_t	$\tau_{b,c}$	
1	✓						Bar diameter reduction according to (1)
2	✓	✓					Pit area (A_{pit}=6.31mm^2) calculated from measured pit penetration. Located at mid-span element.
3	✓	✓	✓				12 % yield strength reduction introduced to elements with pitting corrosion.
4	✓	✓	✓	✓			f_c reduction was quantified separately for the top compression (27.2MPa) and bottom tension (22.9MPa) region.
5	✓	✓	✓	✓		✓	CEB-FIP1990 unconfined concrete bond model with "Good bond conditions" for uncorroded specimen and "All other bond conditions" for corroded specimen
6	✓	✓	✓	✓	✓	✓	C_t parameter controlling exponential decay in the concrete tensile model

Table 1: Modelling variables: U: uniform corrosion, P: pitting corrosion, f_y: yield strength, f_c: concrete compressive strength, C_t: concrete tensile model, $\tau_{b,c}$: bond strength.

Load-deflection results are shown in Figure 6 (left). For the response of beam B111, the concrete tensile strength and initial tangent modulus were estimated as $f_{ct}=0.65f_c^{0.33}$ and $E_c=5000f_c^{0.5}$, which resulted in 2.4MPa and 35,355MPa, respectively. With these values better agreement was found in the crack-development phase. We observed that the curves gradually converge to the experimental response of the corroded beam B116. As expected for flexural failure due to yielding of bottom reinforcement, the maximum load is controlled by uniform and pitting corrosion and reduction in the yield strength. Reduction in the concrete strength has very little influence, and reduction in the bond strength no influence at all provided the failure mode does not change. Bond shows some influence in the post-cracking stiffness prior to initiation of yielding. In Model 6 an additional modification was introduced, which consisted in increasing by a factor of 2 the constitutive model parameter controlling the exponential decay in the tension-stiffening phase of concrete. This is equivalent to reducing the fracture energy by 50%. This last model showed the best overall agreement with the corroded specimen. Failure ultimately occurred due to fracture of bottom reinforcement. Although this was not explicitly modeled, due to lack of data regarding the fracture strain of the reinforcement, calculated tensile strains at ultimate displacement (24mm) were 7.5% at the mid-span steel element, which is close to fracture.

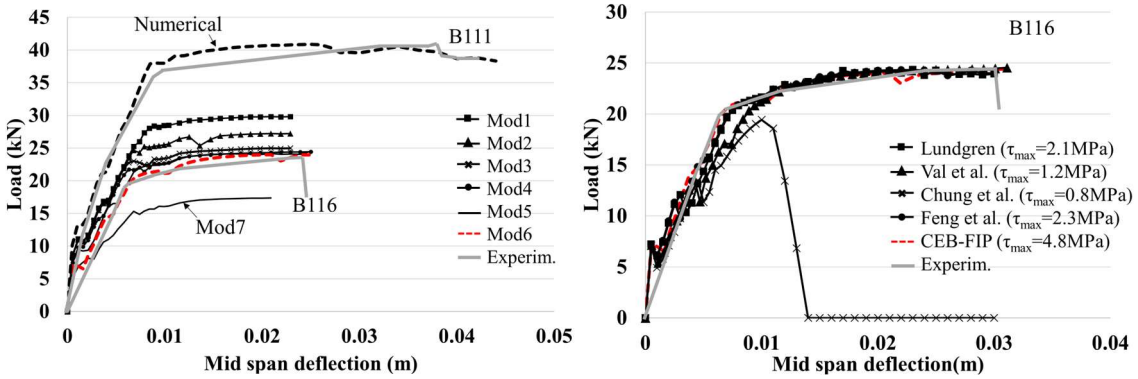

Figure 6: *Left:* Load deflection results for beams B111 (non-corroded reference beam) and B116 (corroded beam); *Right*: sensitivity results for beam B116 comparing different models for degradation of bond between reinforcement and concrete under corrosion

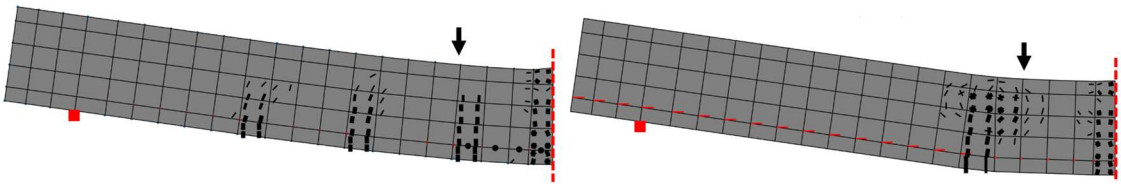

Figure 7. Crack patterns in corroded beam B116 at flexural failure (left) and at bond-slip failure (right).

Model 7 represents the extreme situation in which the top cover elements were completely removed from the numerical model, assuming total spalling of concrete cover. This situation is very conservative, underestimating the collapse load by 30%.

The effect of bond strength is shown in Figure 6 (right). The results discussed so far used the CEB-FIP1990 bond model for unconfined concrete and all other bond conditions. Values for the maximum corroded bond strength using expressions from section 2.3 ranged between 0.8-2.3 MPa. As previously stated, bond mostly affects the post-cracking phase, with negligible influence on the collapse load provided a switch in the failure mode does not occur. For the Cheng et al. model, a pull-out/splitting failure of the bottom flexural reinforcement occurs, which results in an undesirable brittle failure mode at about 20% of the failure load at flexural yielding. Crack patterns reported in Figure 7 show that a single vertical crack develops to the left of the applied load. Limited crack propagation occurs in the case of pull-out/splitting failure, whereas several vertical cracks develop in the case of flexural yielding failure.

4 CONCLUSIONS.

Numerical FE results for flexure-critical beams controlled by yielding of tensile reinforcement indicated that corrosion-induced degradation of reinforcement (area and yield strength) amounts to 95% of the total load reduction. These mechanisms can be regarded as primary mechanisms. Secondary mechanisms, such as reduction in the concrete compressive strength and bond, were found to have a smaller influence. However, under significant degradation secondary mechanisms can become dominant, producing a switch in the failure mode from ductile to brittle. Therefore, both primary and secondary mechanisms should be considered for adequate serviceability and ultimate limit state assessment.

5 REFERENCES.

Angst, U, 2018, “Challenges and opportunities in corrosion of steel in concrete” Materials and Structures 51:4

Apostolopoulos, C.A., Papadakis, V.G., 2008, “Consequences of steel corrosion on the ductility properties of reinforcement bar”, Construction and Building Materials, 22, 2316-2324.

Belarbi, A., Hsu, T., 1995, “Constitutive Laws of Softened Concrete in Biaxial Tension-Compression”, ACI Journal, Vol. 92, n5, Sept-Oct.

Cairns, J, Plizzari, G.A., Du, Y., Law, D.W., Franzoni, C., 2005, “Mechanical properties of corrosion damaged reinforcement”, ACI Material Journal, 102(4), 256-64.

Castel, A., François, R., Arliguie, G., 2000, “Mechanical behavior of corroded reinforced concrete beams - Part 1: Experimental study of corroded beams”, Materials and Structures, 33, 539-544.

CEB-FIP, 1993, “CEB-FIP Model Code 1990”, Bulletin d’information 213/214. Lausanne, Switzerland, 437pp.

Chung, L., Cho, S.-H., Kim, J.-H. J. and Yi, S.T., 2004, “Correction Factor Suggestion for ACI Development Length Provisions Based on Flexural Testing of RC Slabs with Various Levels of Corroded Reinforcing Bars”. Engineering Structures, 26(8), 1013-1026

Coronelli, D., Gambarova, P., 2004, "Structural Assessment of Corroded Reinforced Concrete Beams: Modeling Guidelines ", Journal of Structural Engineering, ASCE, Vol.130, N°8:1214-1224, August.

Darmawan, M.S., Stewart, M.G., 2006, "Effect of Spatially Variable Pitting Corrosion on Structural Reliability of Prestressed Concrete Bridge Girders", Australian Journal of Structural Engineering, 6:2, 147-158.

Feng, Q., Visintin, P., Oehlers D.J., 2006, "Deterioration of bond–slip due to corrosion of steel reinforcement in reinforced concrete", Magazine of Concrete Research, Vol. 68, Issue 15, August, pp. 768-781

fib Bulletin N°10, 2000, "Bond of reinforcement in concrete. State of the art report", fédération internationale du béton (fib). Lausanne, Switzerland.

Fischer, C., 2012, "Auswirkungen der Bewehrungskorrosion auf den Verbund zwischen Stahl und Beton"., Dissertation, Institut für Werkstoffe im Bauwesen der Universität Stuttgart.

Gehlen, C., Mayer TF., von Greve Dierfeld, S., 2012, „Lebensdauerbemessung", Beton-Kalender 2011, (229-278).

Gonzalez, J.A, Andrade C., Alonso, C., Feliu, S., 2011, "Comparison of rates of general corrosion and maximum pitting penetration on concrete embedded steel reinforcement", Cement and Concrete Research, Vol.25, N°2:257-264.

Hanjari, Z.K., Kettil, P., Lundgren, K., 2011, "Analysis of Mechanical Behavior of Corroded Reinforced Concrete Structures", ACI Structural Journal, Vol.108, N°5:532-541, September-October.

IDEEA3D: Nonlinear FEA Software, 2016. Available at: https://sites.google.com/site/ideeanalysis/ .

Lundgren, K., Kettil, P., Hanjari, K., Schlune, H., San Roman, A.S., 2009, "Analytical Model for the Bond-Slip Behavior of Corroded Ribbed Reinforcement", Structure and Infrastructure Engineering, Vol.8, Issue2, pp.157-169.

Maaddawy, T., Soudki, K., Topper, T., 2005, "Analytical Model to Predict Nonlinear Flexural Behavior of Corroded Reinforced Concrete Beams", ACI Structural Journal, 102(4), 550-559.

Molina, F.J, Alonso, C., Andrade, C., 1993, "Cover cracking as a function of rebar corrosion 2 – Numerical model", Materials and Structures, Vol.26, N°163, 532-548.

Morinaga, S., 1996, "Remaining life of reinforced concrete structures after corrosion cracking", In Durability of Buildings Materials and Components, (S Jostrom C (ed)), E&FN Spon, London, UK, pp127-137.

Norm SIA 269, "Grundlagen der Erhalten von Tragwerken", Schweizerischer Ingenieur- und Architektenverein, Ausgabe 2011.

Rodriguez, J., Ortega, L.M., Casal, J., 1997, "Load carrying capacity of concrete structures with corroded reinforcement", Construction and Building Materials, 11(4), 239-248.

Stewart, M.G., Al-Harthy, A., 2008, "Pitting corrosion and structural reliability of corroding RC structures: Experimental data and probabilistic analysis", Reliability Engineering and System Safety, 93, 373-382.

Val, D., Stewart, M.G. and Melchers, R.E., 1998, "Effect of reinforcement corrosion on reliability of highway bridges", Engineering Structures, Vol.20, No. 11, pp. 1010-1019.

Val, D.V., Melchers, R.E., 1997, "Reliability of deteriorating RC slab bridges", Journal of Structural Engineering, ASCE, 123(12), 1638-44.

Vecchio, F., Collins, M., 1986, "The modified compression field theory for RC elements subjected to shear", ACI Journal, n9, 82-S22.

Vidal, T., Castel, A., Francois, R., 2004, "Analyzing crack width to predict corrosion in reinforced concrete", Cement and Concrete Research, Vol.34, 165-174.